Radiation Physics and Chemistry 212 (2023) 111120

Contents lists available at ScienceDirect

Radiation Physics and Chemistry

journal homepage: www.elsevier.com/locate/radphyschem

Gamma, charged particle and neutron radiation shielding capacities of ternary composites having polyester/barite/tungsten boride

F. Akman [a,b,*], H. Ozdogan [c], O. Kilicoglu [d], H. Ogul [e], O. Agar [f], M.R. Kacal [g], H. Polat [h], A. Tursucu [i]

[a] Bingöl University, Vocational School of Social Sciences, Department of Property Protection and Security, Program of Occupational Health and Safety, 12000, Bingöl, Turkiye
[b] Bingöl University, Central Laboratory Application and Research Center, 12000, Bingöl, Turkiye
[c] Antalya Bilim University, Vocational School of Health Services, Akdeniz Blv. No: 90, 07085, Antalya, Turkiye
[d] Vocational School of Health Services, Marmara University, Kartal, İstanbul, Turkiye
[e] Sinop University, Faculty of Engineering and Architecture, Department of Nuclear Engineering, Sinop, Turkiye
[f] Karamanoğlu Mehmetbey University, Department of Medical Imaging Techniques, 70100, Karaman, Turkiye
[g] Giresun University, Arts and Sciences Faculty, Department of Physics, 28100, Giresun, Turkiye
[h] Bingöl University, Vocational School of Technical Sciences, Department of Architecture and Urban Planning, 12000, Bingöl, Turkiye
[i] Şırnak University, Engineering Faculty, Department of Electrical and Electronics Engineering, 73000, Sirnak, Turkiye

ARTICLE INFO

Keywords:
Barit
Tungsten boride
Shielding efficiency
Gamma-ray spectrometer
Monte-Carlo codes

ABSTRACT

The presented work investigates the photon, charged particle and neutron radiation shielding performances of polyester-based composites filled with barite and/or tungsten boride by using experimental, theoretical, and Monte Carlo simulation techniques. The amount of barite/tungsten boride varying from 0 wt% to 50 wt% in the material and polyester resin were exploited as filler and base materials, respectively. Experimental evaluation of BaWB composites has been performed with help of an HPGe detector based gamma spectrometer as well as ^{22}Na, ^{133}Ba, ^{137}Cs and ^{60}Co radioactive point sources with energies in the range of 276.4–1332.5 keV. The experimental data were compared to those theoretically calculated in WinXCOM as well as Monte Carlo (MC) simulations, i.e., MCNP6, GEANT4 and FLUKA codes. The obtained mass attenuation coefficients for the produced composites were in good agreement with the results of MC simulations and WinXCOM software. Comparing to the other polymer composite samples, the sample with the maximum tungsten boride weight percentage has the best radiation shielding property because of having the highest attenuation coefficients and lowest absorption thicknesses.

1. Introduction

Since its discovery, radiation has started to be widely used in many fields, especially in medical applications. It was first used for the diagnosis of diseases by taking advantage of the absorption feature of X-rays. Later, it was used in the treatment of diseases, including internal and external radiotherapy. The use of ionizing radiation has expanded with the advancement of science, technology, and industry. While the usage of radiation has expanded, the necessity of radiation protection against its harmful effects has also started to become crucial. In order to avoid from the harmful effects of ionizing radiation, it is necessary to pay attention to three parameters: time, distance, and shielding. Therefore, it could be safely stated that minimum exposure time, maximum distance to the radiation source and using shielding materials are vital in the radiation environment. The rule that aims to eliminate the effect of the dose by placing the material between the radiation source and the people exposed to the dose caused by the source is called the shielding rule. In order to be protected from the harmful effects of ionizing radiation, it is necessary to determine the radiation shielding properties of the materials used in radiation centers beforehand. Experimental techniques or theoretical and simulation methods have to be utilized in order to determine the used shielding materials.

There are many different shielding materials that are used for radiation protection. These shielding materials are generally chosen taking

* Corresponding author. Bingöl University, Vocational School of Social Sciences, Department of Property Protection and Security, Program of Occupational Health and Safety, 12000, Bingöl, Turkiye.
E-mail address: fakman@bingol.edu.tr (F. Akman).

https://doi.org/10.1016/j.radphyschem.2023.111120
Received 14 February 2023; Received in revised form 11 April 2023; Accepted 11 June 2023
Available online 14 June 2023

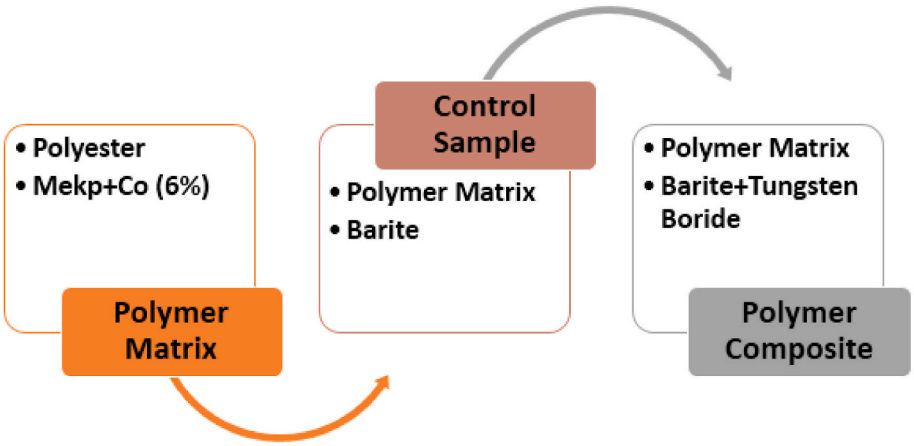

Fig. 1. Production stage of polymer composites.

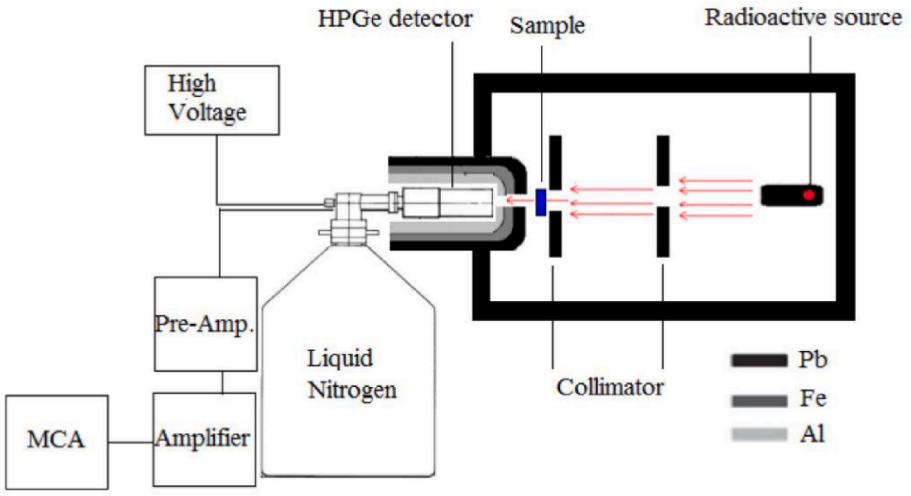

Fig. 2. Experimental arrangement.

Table 1
The chemical contents and densities for the prepared composites.

Sample Code	Compositions (%)								Exp.	Theo.
	H	B	C	O	S	Co	Ba	W	ρ (g/cm^3)	ρ (g/cm^3)
BaWB-0	0.9025	–	12.1200	28.9989	10.9746	0.0024	47.0017	–	2.7325	2.8002
BaWB-10	0.9025	0.4417	12.1200	26.8182	9.8820	0.0024	42.3224	7.5108	2.8153	2.9016
BaWB-20	0.9025	0.8873	12.1200	24.6181	8.7797	0.0024	37.6013	15.0887	2.8962	3.0115
BaWB-30	0.9025	1.3310	12.1200	22.4277	7.6822	0.0024	32.9012	22.6331	3.0454	3.1223
BaWB-40	0.9025	1.7746	12.1200	20.2373	6.5848	0.0024	28.2010	30.1774	3.1185	3.2574
BaWB-50	0.9025	2.2183	12.1200	18.0469	5.4873	0.0024	23.5008	37.7218	3.2775	3.3948

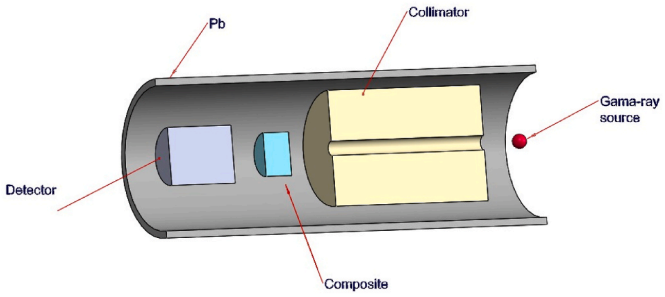

Fig. 3. Simulation arrangement.

radiation type into account. For example, the materials prepared to keep the photon radiation are generally constructed from high atomic number of elements. Although lead is the most used shielding material for photon radiation, researchers are working on different shielding materials such as composites (Medhat and Singh, 2014; Singh and Mudahar, 1992; Singh et al., 2007; Baştuğ et al., 2011), building materials (Çakıroğlu et al., 2021; Tekin, 2016; Shirmardi et al., 2013), glasses (Al-Hadeethi et al., 2019; Aloraini et al., 2021; Alqahtani et al., 2021; Ozdogan et al., 2022a; Şekerci et al., 2019), etc. On this regard, Alavian et al. (Alavian and Tavakoli-Anbaran, 2019) investigated the shielding properties of light-density polyethylene reinforced with tungsten particles by using Monte Carlo simulations. Besides, in another work, the radiation shielding properties of fiber-reinforced polymer composites

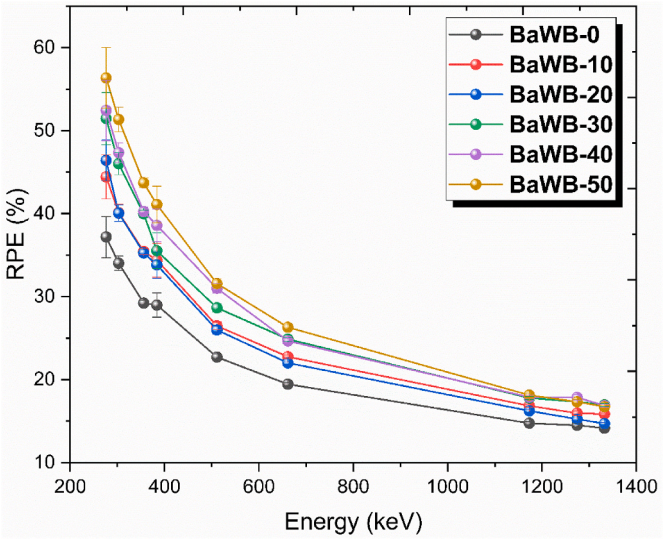

Fig. 4. RPE values versus photon energy for the prepared composites.

incorporating lead nanoparticles were calculated by using the MCNP code (Abu Saleem RAbdelal et al., 2021). Additionally, various gamma shielding parameters, such as mass attenuation coefficients (MAC), energy absorption effective atomic number (ZPEA), electron density, of nylon, poly-acrylo-nitrile, poly-methyl-acrylate, poly-vinyl-chloride, poly-styrene, synthetic rubber, and poly-tetra-fluro-ethylene from 1 keV to 20 MeV were studied by Singh et al. (2010). In another study, photon shielding properties of some silicon polymers and coordination polymers were measured at the photon energies of 81, 276, 302.8, 356, 383.80, 511, 662, 835, 1173 and 1332 keV by using Ba-133, Na-22, Cs-137, Mn-54 and Co-60 sources (Nagaraja et al., 2022). Wahabi et al. (Vahabi et al., 2017) were computed radiation shielding properties of some polymers (Perspex, Poly-carbonate, and PMMA) by using MCNP code.

Unlike photon shielding materials, neutron shielding materials are constructed from low atomic number elements (H, B, C, O, etc). Concrete and water tanks are the most common materials used at high energy neutron shielding applications while paraffin and polyethylene are generally used materials at low energy neutron shielding. Generally, the elements which have high neutron capture cross-sections such as Boron, Cadmium, and Gadolinium are used for neutron shielding. The effects of the secondary photon dose produced from the (n, γ) reaction could be reduced by using boron in the shielding material. Recently, researchers have investigated new shielding materials to prevent people from neutron radiation. Gong et al. (2018) have determined neutron shielding properties of some concretes by using Monte Carlo simulation techniques. In another study neutron flux and dose were calculated for cement concrete which is the main component of shielding material of nuclear power plants (Piotrowski et al., 2012). Besides, the comparisons of neutron and photon shielding effectiveness of materials, composed of polyethylene, borated polyethylene, lithium-filled polyethylene, lead, and iron were further studied by Štekl et al. (2000)

In the presented study, photon, charged and neutron attenuation properties of polyester-based composites reinforced with barite and/or tungsten boride have been investigated by using experimental, theoretical, and Monte Carlo simulation codes. MACs, half value layer (HVL), and Z_{eff} have been measured at 276.4, 302.9, 356.0, 383.9, 511.0, 661.7, 1173.2, 1274.5, and 1332.5 keV photon energies by using HPGE detector. In addition to the experimental process, theoretical calculations of WinXCOM and MCNP6, GEANT4, and FLUKA which are Monte Carlo-based codes have been employed for photon shielding properties. Also, neutron transmission, mean free path, and total macroscopic cross-section have been calculated to conduct a proper discussion on the

Table 2
μ/ρ ($cm^2\ g^{-1}$) results for the prepared composites.

Energy (keV)	BaWB-0					BaWB-10					BaWB-20				
	Exp.	WinX.	MCNP6	GEANT4	FLUKA	Exp.	WinX.	MCNP6	GEANT4	FLUKA	Exp.	WinX.	MCNP6	GEANT4	FLUKA
276.4	0.1577 ± 0.0110	0.1614	0.1624	0.1537	0.1610	0.1719 ± 0.0108	0.1768	0.1776	0.1680	0.1763	0.1939 ± 0.0109	0.1923	0.1930	0.1822	0.1917
302.9	0.1411 ± 0.0046	0.1451	0.1456	0.1380	0.1447	0.1501 ± 0.0049	0.1572	0.1581	0.1494	0.1568	0.1590 ± 0.0051	0.1694	0.1699	0.1633	0.1689
356.0	0.1172 ± 0.0027	0.1232	0.1236	0.1178	0.1229	0.1281 ± 0.0029	0.1310	0.1314	0.1249	0.1306	0.1351 ± 0.0031	0.1390	0.1392	0.1329	0.1387
383.9	0.1161 ± 0.0063	0.1151	0.1155	0.1109	0.1148	0.1234 ± 0.0077	0.1215	0.1219	0.1165	0.1211	0.1283 ± 0.0065	0.1280	0.1283	0.1224	0.1276
511.0	0.0874 ± 0.0023	0.0923	0.0929	0.0899	0.0922	0.0900 ± 0.0024	0.0953	0.0956	0.0928	0.0952	0.0935 ± 0.0025	0.0984	0.0987	0.0955	0.0981
661.7	0.0734 ± 0.0016	0.0781	0.0785	0.0772	0.0780	0.0756 ± 0.0017	0.0796	0.0800	0.0783	0.0794	0.0773 ± 0.0017	0.0812	0.0814	0.0794	0.0810
1173.2	0.0541 ± 0.0013	0.0564	0.0567	0.0559	0.0563	0.0540 ± 0.0013	0.0566	0.0570	0.0561	0.0565	0.0551 ± 0.0013	0.0568	0.0572	0.0562	0.0568
1274.5	0.0532 ± 0.0014	0.0539	0.0545	0.0538	0.0538	0.0509 ± 0.0013	0.0541	0.0544	0.0539	0.0539	0.0514 ± 0.0013	0.0542	0.0547	0.0542	0.0541
1332.5	0.0518 ± 0.0012	0.0526	0.0532	0.0528	0.0525	0.0505 ± 0.0011	0.0528	0.0534	0.0530	0.0527	0.0494 ± 0.0011	0.0529	0.0535	0.0527	0.0528
Energy (keV)	BaWB-30					BaWB-40					BaWB-50				
	Exp.	WinX.	MCNP6	GEANT4	FLUKA	Exp.	WinX.	MCNP6	GEANT4	FLUKA	Exp.	WinX.	MCNP6	GEANT4	FLUKA
276.4	0.2057 ± 0.0133	0.2078	0.2081	0.1966	0.2070	0.2099 ± 0.0152	0.2233	0.2240	0.2140	0.2225	0.2259 ± 0.0153	0.2387	0.2389	0.2256	0.2379
302.9	0.1755 ± 0.0062	0.1815	0.1820	0.1737	0.1809	0.1812 ± 0.0058	0.1936	0.1940	0.1848	0.1929	0.1962 ± 0.0069	0.2058	0.2063	0.1937	0.2051
356.0	0.1454 ± 0.0033	0.1469	0.1475	0.1399	0.1462	0.1454 ± 0.0035	0.1548	0.1551	0.1462	0.1541	0.1565 ± 0.0037	0.1627	0.1629	0.1535	0.1619
383.9	0.1249 ± 0.0080	0.1345	0.1348	0.1285	0.1340	0.1377 ± 0.0076	0.1410	0.1417	0.1338	0.1406	0.1442 ± 0.0082	0.1474	0.1478	0.1397	0.1469
511.0	0.0961 ± 0.0025	0.1014	0.1017	0.0982	0.1010	0.1048 ± 0.0029	0.1044	0.1045	0.1008	0.1040	0.1034 ± 0.0028	0.1075	0.1076	0.1031	0.1070
661.7	0.0815 ± 0.0018	0.0827	0.0829	0.0808	0.0824	0.0800 ± 0.0018	0.0842	0.0844	0.0820	0.0838	0.0832 ± 0.0018	0.0857	0.0858	0.0834	0.0854
1173.2	0.0558 ± 0.0013	0.0571	0.0573	0.0566	0.0570	0.0557 ± 0.0013	0.0573	0.0575	0.0566	0.0572	0.0545 ± 0.0013	0.0576	0.0578	0.0567	0.0574
1274.5	0.0541 ± 0.0014	0.0544	0.0548	0.0542	0.0543	0.0556 ± 0.0015	0.0546	0.0550	0.0542	0.0544	0.0518 ± 0.0014	0.0548	0.0551	0.0542	0.0547
1332.5	0.0529 ± 0.0012	0.0531	0.0536	0.0528	0.0530	0.0522 ± 0.0012	0.0533	0.0537	0.0530	0.0531	0.0499 ± 0.0011	0.0534	0.0538	0.0532	0.0533

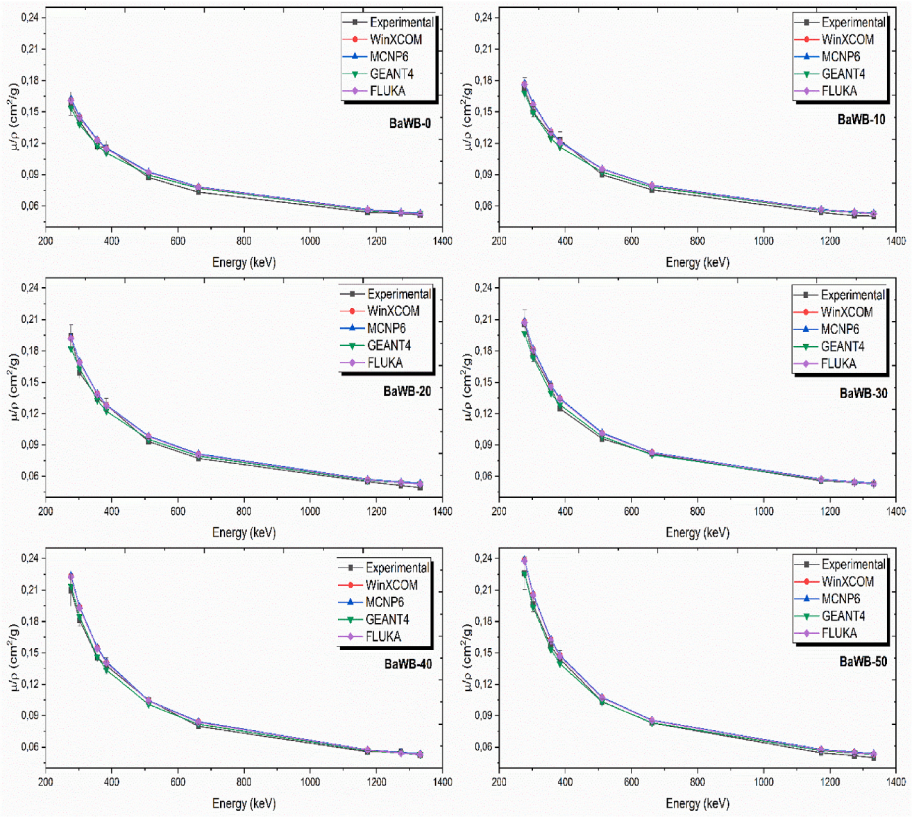

Fig. 5. μ/ρ values versus photon energy for the prepared composites.

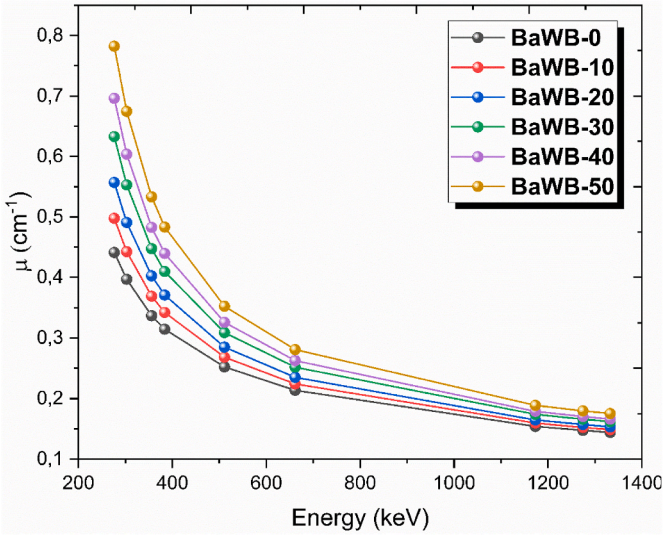

Fig. 6. μ values versus photon energy for the prepared composites.

neutron shielding capacities. In addition to radiation shielding properties of charged particles, alpha and proton stopping powers have been further computed.

2. Materials and method

2.1. Preparation

Materials formed by combining two or more materials with superior properties in a single material or combining them at a macro level in order to reveal a new feature are called composite materials. Polymer concrete is a composite material consisting of resin and hardener in a continuous polymer matrix, supported by a filler material that hardens with chemical reaction. The composite production process was carried out in three different stages. In the first stage, polymer matrix was obtained by mixing $C_{16}O_7H_{14}$ (unsaturated polyester resin), $C_8O_6H_{18}$ (methyl ethyl ketone peroxide, MEKP) as hardener and $CoC_{16}H_{30}O_4$ (cobalt octoate (6%)) as reaction accelerator. In the second step, the control sample was produced by adding the unsaturated polymer resin and barite mineral as a filling material into the polymer matrix. In the third stage, polymer composite samples were obtained by keeping the polymer matrix amount constant in the produced samples and replacing the barite mineral with tungsten boride at the rate of 10%, 20%, 30%, 40% and 50% by weights. The production stage of polymer composites is given in Fig. 1.

2.2. Theoretical basis

Shielding research and simulation studies are widely used to evaluate gamma-ray shielding factors in order to choose the best material available (Kilicoglu and Mehmetcik, 2021). In this work, the photon shielding properties of six different composite samples were studied. The following equation computes the mass attenuation coefficient (MAC) in cm^2/g. It is linked to density, and linear attenuation coefficient (LAC) expressed in the Beer-Lambert rule.

$$\mu/\rho = \frac{1}{\rho x}\ln\left(\frac{I}{I_0}\right) \quad (1)$$

where, I and I_0 represent the transmitted and the original intensities of photons, respectively. μ represents the LAC parameter, ρ represents the density of the material and x represents the thickness of the absorber. On the other hand, the mixture rule computes the total MAC of any mixture, or a composite made up of several elements, taking into consideration

Table 3
HVL (cm) results for the prepared composites.

Energy (keV)	BaWB-0		BaWB-10		BaWB-20		BaWB-30		BaWB-40		BaWB-50	
	Exp.	Theo.	Exp.	Theo.	Exp.	Theo.	Exp.	Theo.	Exp.	Theo.	Exp.	Theo.
276.4	1.608 ± 0.112	1.572	1.432 ± 0.090	1.393	1.234 ± 0.069	1.244	1.106 ± 0.071	1.095	1.059 ± 0.077	0.996	0.936 ± 0.064	0.886
302.9	1.798 ± 0.058	1.748	1.640 ± 0.053	1.566	1.505 ± 0.048	1.413	1.297 ± 0.046	1.254	1.226 ± 0.039	1.148	1.078 ± 0.038	1.028
356.0	2.164 ± 0.049	2.060	1.922 ± 0.044	1.879	1.771 ± 0.041	1.722	1.565 ± 0.036	1.550	1.528 ± 0.037	1.436	1.352 ± 0.032	1.300
383.9	2.185 ± 0.118	2.204	1.996 ± 0.124	2.026	1.866 ± 0.095	1.869	1.822 ± 0.117	1.692	1.614 ± 0.089	1.577	1.467 ± 0.084	1.434
511.0	2.903 ± 0.078	2.748	2.736 ± 0.074	2.583	2.560 ± 0.069	2.433	2.368 ± 0.063	2.244	2.120 ± 0.058	2.128	2.046 ± 0.056	1.968
661.7	3.457 ± 0.076	3.246	3.257 ± 0.072	3.091	3.098 ± 0.068	2.949	2.794 ± 0.062	2.754	2.779 ± 0.061	2.641	2.543 ± 0.057	2.469
1173.2	4.685 ± 0.108	4.501	4.558 ± 0.106	4.351	4.347 ± 0.101	4.211	4.082 ± 0.095	3.988	3.992 ± 0.092	3.878	3.880 ± 0.090	3.675
1274.5	4.772 ± 0.124	4.707	4.841 ± 0.125	4.554	4.656 ± 0.120	4.412	4.203 ± 0.109	4.182	3.999 ± 0.106	4.071	4.079 ± 0.107	3.861
1332.5	4.902 ± 0.109	4.819	4.873 ± 0.109	4.664	4.845 ± 0.108	4.520	4.303 ± 0.097	4.286	4.259 ± 0.095	4.174	4.240 ± 0.095	3.960

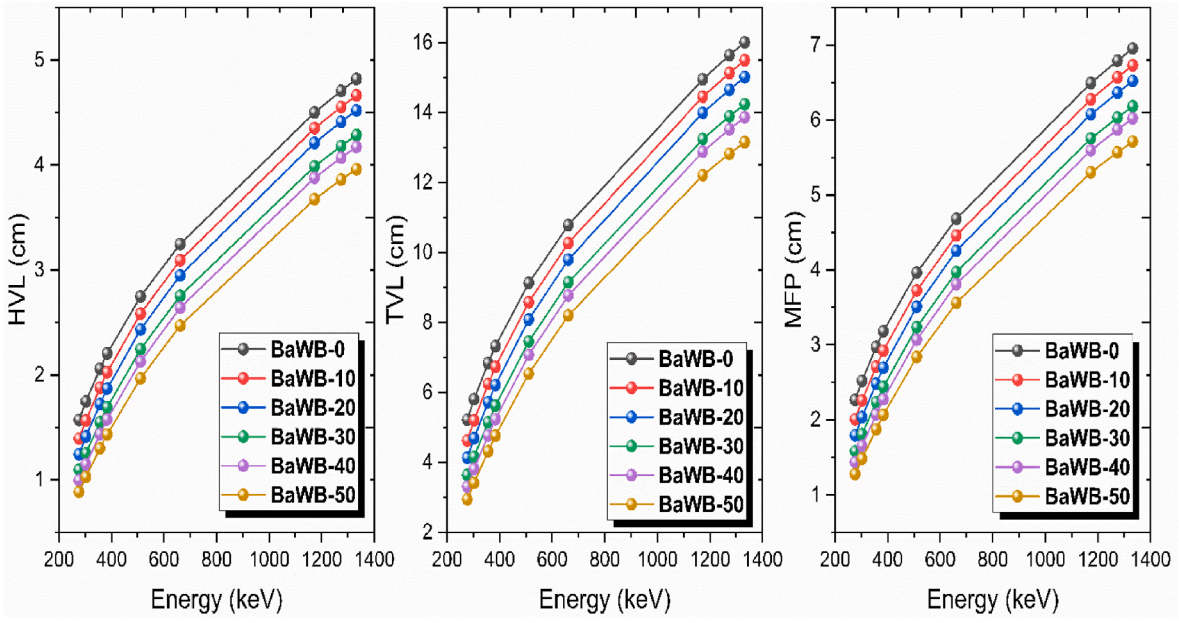

Fig. 7. HVL, TVL and MFP values versus photon energy for the prepared composites.

the contribution rates in the mixed material.

$$\left(\frac{\mu}{\rho}\right)_{composite} = \sum W_i \left(\frac{\mu}{\rho}\right)_i \tag{2}$$

where W_i and $(\mu/\rho)_i$ indicate the weight fraction and mass attenuation coefficient of i.th element in composites. Half Value Layer (HVL, cm), Tenth Value Layer (TVL, cm), and Mean Free Path (MFP, cm) indicate the thickness of the sample needed to lower photon intensity to 50%, 90% and 36.8% respectively (Ozdogan et al., 2022b; Kilicoglu et al., 2022). These parameters are determined using the following equations (3)–(5) in order; they are all dependent on the relevant material's LAC.

$$HVL = \frac{ln\,2}{\mu} \tag{3}$$

$$TVL = \frac{\ln 10}{\mu} \tag{4}$$

$$MFP = \frac{1}{\mu} \tag{5}$$

The important factor in establishing the shielding effectiveness of any combination is the effective atomic number (Z_{eff}), a dimensionless quantity that is stated as follows.

$$Z_{eff} = \frac{\sum_i f_i A_i \left(\frac{\mu}{\rho}\right)_i}{\sum_j f_j \frac{A_j}{Z_j} \left(\frac{\mu}{\rho}\right)_j} \tag{6}$$

where f_i represents the fractional abundance of the relative element in the composite, A_i and Z_j represent the atomic weight and number, respectively (Kilicoglu et al., 2021; Kilicoglu, 2019).

An important factor that determines a shielding material's effectiveness is the radiation protection efficiency, which is stated as follows:

$$RPE = \left(1 - \frac{I}{I_0}\right) \times 100 \tag{7}$$

Table 4
Z_{eff} results for the prepared composites.

Energy (keV)	BaWB-0		BaWB-10		BaWB-20		BaWB-30		BaWB-40		BaWB-50	
	Exp.	Theo.	Exp.	Theo.	Exp.	Theo.	Exp.	Theo.	Exp.	Theo.	Exp.	Theo.
276.4	14.641 ± 1.020	14.982	16.078 ± 1.009	16.535	18.275 ± 1.025	18.126	19.538 ± 1.262	19.734	20.091 ± 1.457	21.367	21.787 ± 1.479	23.026
302.9	13.810 ± 0.448	14.204	14.849 ± 0.483	15.555	15.906 ± 0.509	16.948	17.757 ± 0.624	18.366	18.546 ± 0.591	19.816	20.308 ± 0.717	21.300
356.0	12.515 ± 0.285	13.148	13.887 ± 0.315	14.208	14.890 ± 0.341	15.313	16.281 ± 0.373	16.448	16.558 ± 0.398	17.621	18.115 ± 0.433	18.834
383.9	12.881 ± 0.695	12.767	13.927 ± 0.868	13.718	14.740 ± 0.750	14.712	14.619 ± 0.936	15.737	16.413 ± 0.908	16.801	17.506 ± 1.001	17.905
511.0	11.149 ± 0.298	11.778	11.738 ± 0.316	12.432	12.469 ± 0.336	13.123	13.121 ± 0.347	13.843	14.651 ± 0.400	14.597	14.797 ± 0.403	15.388
661.7	10.595 ± 0.233	11.284	11.182 ± 0.247	11.783	11.719 ± 0.257	12.311	12.677 ± 0.280	12.865	12.780 ± 0.282	13.448	13.651 ± 0.303	14.063
1173.2	10.377 ± 0.240	10.801	10.632 ± 0.247	11.140	11.140 ± 0.259	11.500	11.607 ± 0.271	11.880	11.933 ± 0.276	12.282	12.036 ± 0.280	12.709
1274.5	10.636 ± 0.276	10.783	10.453 ± 0.270	11.112	10.863 ± 0.280	11.463	11.773 ± 0.306	11.833	12.442 ± 0.329	12.224	11.962 ± 0.314	12.640
1332.5	10.596 ± 0.237	10.777	10.628 ± 0.237	11.103	10.683 ± 0.239	11.450	11.771 ± 0.264	11.816	11.960 ± 0.267	12.204	11.781 ± 0.263	12.615

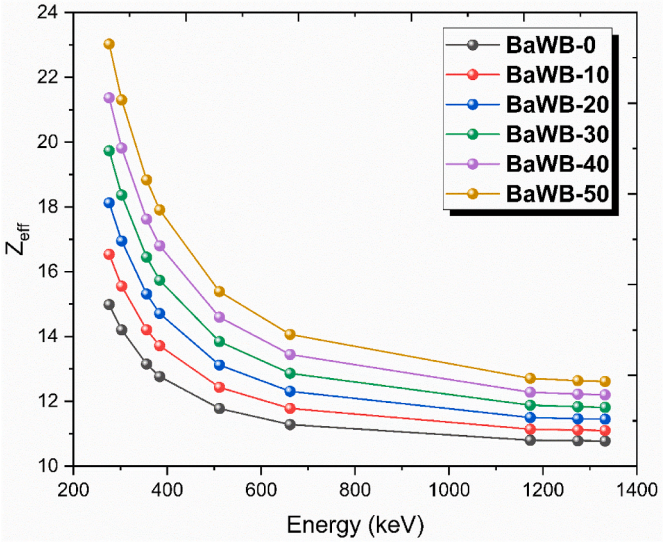

Fig. 8. Z_{eff} values versus photon energy for the prepared composites.

The prepared samples' neutron removal cross sections were computed using the mixing rule. Formulas (8-9) provide the equations for the mass removal and neutron removal cross sections.

$$\sum_R = \sum_i \rho_i \left(\sum_{R/\rho} \right)_i \tag{8}$$

$$\sum_{R/\rho} = \sum_i w_i \left(\sum_{R/\rho} \right)_i \tag{9}$$

where w_i is the weight ratio and ρ_i is the partial density of the elements (Kara et al., 2020a).

The SRIM (Stopping and Range of Ions in Matter) software tools were used to simulate the amounts of energy lost and the rates of particle

Table 6
Total macroscopic cross sections, mean free paths and number of transmitted neutrons of 10 mm thickness sample and 10^7 neutrons at 4.5 MeV for the produced composites.

Sample	Total macroscopic cross section (cm^{-1})	Mean free path (mm)	Number of transmitted neutrons
BaWB-0	2.0459	4.8878	8713484
BaWB-10	2.0460	4.8874	8700237
BaWB-20	2.0461	4.8872	8687140
BaWB-30	2.0494	4.8794	8646862
BaWB-40	2.0501	4.8779	8640665
BaWB-50	2.0515	4.8745	8601998

Table 5
Effective removal cross section results for the produced composites.

Element	BaWB-0 (ρ = 2.7325 g cm^{-3})		BaWB-10 (ρ = 2.8153 g cm^{-3})		BaWB-20 (ρ = 2.8962 g cm^{-3})		BaWB-30 (ρ = 3.0454 g cm^{-3})		BaWB-40 (ρ = 3.1185 g cm^{-3})		BaWB-50 (ρ = 3.2775 g cm^{-3})	
	Partial density	Σ_R (cm^{-1})	Partial density	Σ_R (cm^{-1})	Partial density	Σ_R (cm^{-1})	Partial density	Σ_R (cm^{-1})	Partial density	Σ_R (cm^{-1})	Partial density	Σ_R (cm^{-1})
H	0.024662	0.014748	0.025408	0.015194	0.026139	0.015631	0.027486	0.016436	0.028146	0.016831	0.029580	0.017689
B	–	–	0.012435	0.000715	0.025698	0.001478	0.040533	0.002331	0.055342	0.003182	0.072704	0.004180
C	0.331181	0.016625	0.341209	0.017129	0.351016	0.017621	0.369101	0.018529	0.377965	0.018974	0.397230	0.019941
O	0.792401	0.032092	0.755003	0.030578	0.712984	0.028876	0.683013	0.027662	0.631106	0.025560	0.591485	0.023955
S	0.299883	0.008307	0.278205	0.007706	0.254275	0.007043	0.233954	0.006481	0.205348	0.005688	0.179845	0.004982
Co	0.000065	0.000001	0.000067	0.000001	0.000069	0.000001	0.000073	0.000001	0.000074	0.000001	0.000078	0.000002
Ba	1.284331	0.016568	1.191487	0.015370	1.089003	0.014048	1.001972	0.012925	0.879457	0.011345	0.770236	0.009936
W	–	–	0.211450	0.002326	0.436997	0.004807	0.689268	0.007582	0.941092	0.010352	1.236326	0.013600
Total	**2.7325**	**0.0883**	**2.8153**	**0.0890**	**2.8962**	**0.0895**	**3.0454**	**0.0919**	**3.1185**	**0.0919**	**3.2775**	**0.0943**

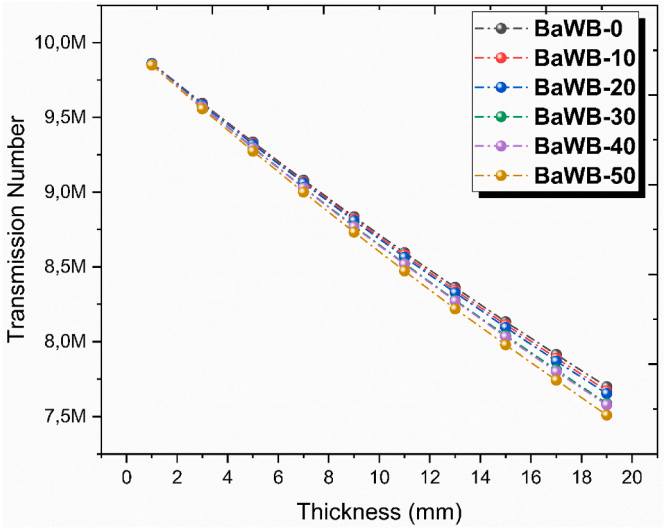

Fig. 9. The transmitted neutron numbers versus sample thicknesses between 1 and 19 mm for the prepared composites.

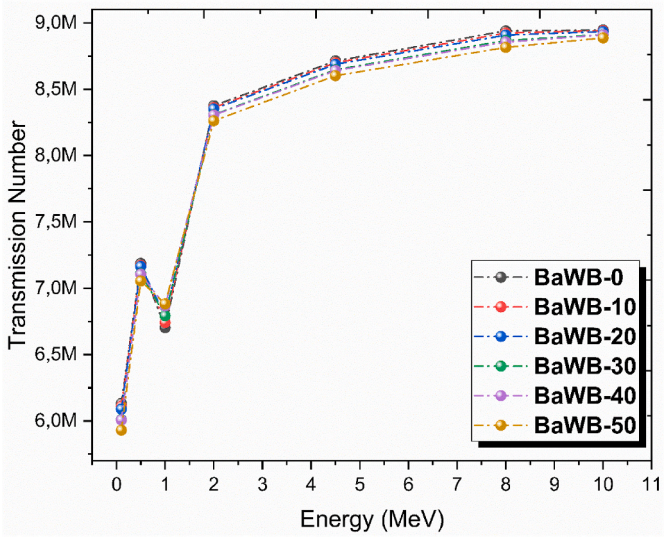

Fig. 10. The transmitted neutron numbers versus neutron energies between 0.1 and 10 MeV for the prepared composites.

damage. It computes many characteristics of ion transport in the matter. Depending on the dose and energy levels, radiation has different effects on different materials. The conventional SRIM code computes using the beam model. Additionally, the disparate SRIM results can be explained by the radiation damage caused by the ions in the material. All particles are thought to be at the same location, angle, and energy level during the SRIM code computation. As a result, without taking into account particle dispersion, the SRIM results reflect the normalized values. On the basis of the SRIM method, the particle beam-which corresponds to the actual experimental setup-was used. Six different materials made from composite samples had their mass stopping power (MSP) values calculated using the SRIM software for energies between 0.015 and 15 MeV. This equation represents the Bethe-Bloch formula for computing MSP values:

$$-\frac{dE}{dx}=\frac{4\pi k_0^2 Z^2 e^4 n}{mc^2\beta^2}\left[ln\frac{2mc^2\beta^2}{I(1-\beta^2)}-\beta^2\right] \tag{10}$$

where the MSP is a function of the ion's mass (m), velocity (β), and charge (e), as well as and density of the material (ρ) and the atomic

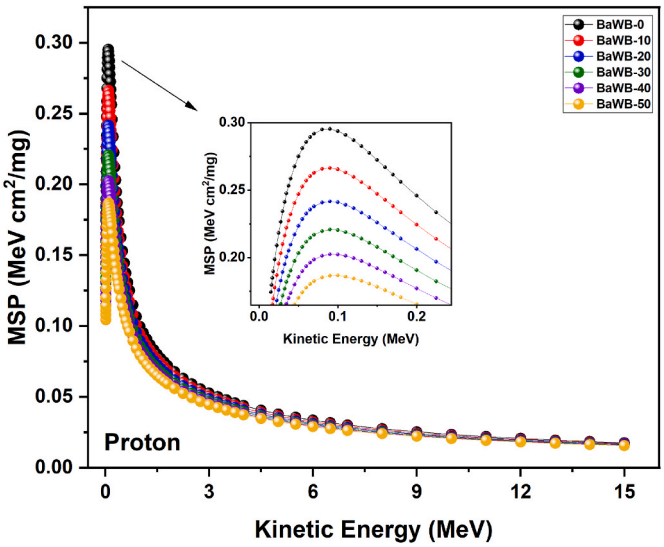

Fig. 11. MSP values versus kinetic energy of proton for the prepared composites.

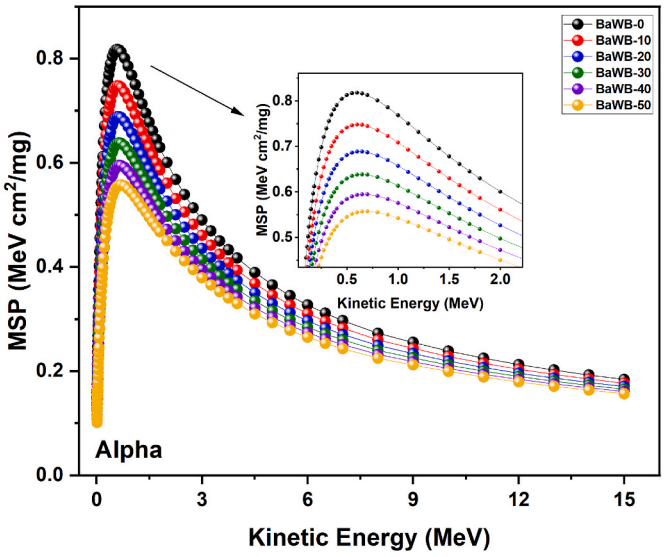

Fig. 12. MSP values versus kinetic energy of alpha for the prepared composites.

number (Z).

While using ionizing radiation, it is crucial to understand the amount of energy lost in charged particles. MSP is a function that represents the loss of kinetic energy and indicates the rate of energy loss for charged particles. The protection offered by the shielding material is revealed by the MSP results. The average distance of an alpha or proton particle's penetration is indicated by its projected range (PR). These computed metrics provide quantifiable evidence of the composite samples' radiation-beam-blocking abilities. The ideal material is assessed at the lowest projected range values for the radiation protection characteristic. In addition, the PR value is a calculation used to understand the charged particle transport patterns. The formula determines PR values.

$$R(\beta)=\left(M/Z^2\right)R_p(\beta) \tag{11}$$

MSP and PR values for both H^1 and He^{+2} particles were estimated in this work using the SRIM algorithm for composite samples with energy ranging from 0.015 to 15 MeV. MSP and PR values have been recognized

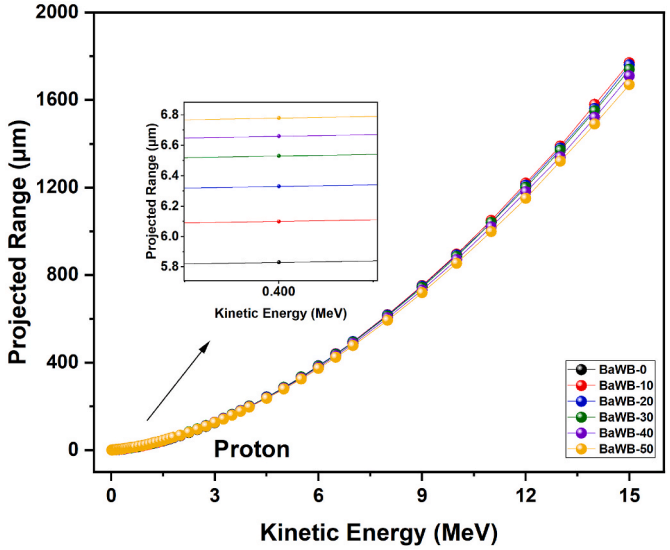

Fig. 13. The projected range values versus kinetic energy of proton for the prepared composites.

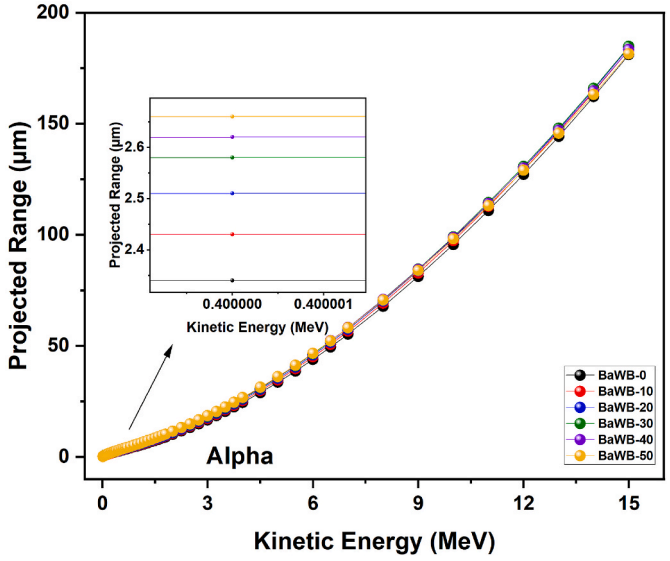

Fig. 14. The projected range values versus kinetic energy of alpha for the prepared composites.

as crucial factors in estimating the level of radiation protection (Alothman et al., 2021; Kara et al., 2020b; Kilicoglu and Tekin, 2020).

2.3. Experimental details

Photons emitting at various photon energies utilizing ^{133}Ba (276.4, 302.9, 356.0 and 383.9 keV), ^{22}Na (511.0 and 1274.5 keV), ^{137}Cs (661.7 keV) and ^{60}Co (1173.2 and 1332.5 keV) radioactive point sources have been detected by gamma ray spectrometer to determine the original and attenuated gamma ray photons for 0%–50% barit/tungsten boride filled composites at Giresun University Radiation Protection Laboratory. The gamma ray measurements have been applied with help of spectrometer equipped with an High Purity Germanium (HPGe) detector (GEM-SP7025P4-B model) as well as an high voltage source of 2600 V with multichannel analyzer (MCA), positive polarity, ternary composites and collimators in geometrical setup as shown in Fig. 2. The distance of the composite to the source and detector window was set to 35 and 28 cm, respectively. The measurements for all samples were repeated three times in order to minimize the statistical error of the conducted experiment. More experimental details are found in previous published works (Akman et al., 2021, 2022).

2.4. Monte Carlo simulations

Mass attenuation characteristic of the shielding materials can be tested by calculating mass attenuation coefficient. Besides experimental results of mass attenuation coefficients, these parameters were simulated by using the WinXCOM (Gerward et al., 2001) program. After entering the chemical composition of the samples into the WinXCOM, mass attenuation results were obtained (see Table 1).

MCNP6, FLUKA and GEANT4 Monte Carlo codes have been employed to evaluate sensitively the photon attenuation performances of BaWB coded samples. The simulations findings have been reported along with those of experimental and WinXCOM results. Transportation of various ionizing radiations like electrons, photons, heavy-ions and neutrons through targets of interest could be simulated with MCNP6 (Goorley et al., 2012), GEANT4 (Agostinelli et al., 2003) and FLUKA (Battistoni et al., 2015) codes. Sketch of the geometry used for the simulations have been shown in Fig. 3. Additionally, more details on codes have been mentioned in our previous works (Ozdogan et al., 2022b; Oğul et al., 2022; Özkalaycı et al., 2020).

3. Results and discussion

The presented study provides some detailed analyses for polyester based composites reinforced with barite and/or tungsten boride. The first considered analysis for the prepared composites is the determination of gamma attenuation characteristics of the chosen materials. In order to conduct a proper discussion on the gamma attenuation parameters, experimental, theoretical and simulation techniques are utilized. In this context, Fig. 4 provides radiation protection efficiency values for each material. The highest efficiency is obtained with BaWB-50 composite, and the efficiency values could be ordered as: BaWB-50 > BaWB-40 > BaWB-30 > BaWB-20 > BaWB-10 > BaWB-0. The difference between the samples is greater at lowest energy and decreases with increase of the energy of the gamma radiation.

Besides the RPE values, Table 2 gives the numerical values for γ coefficients. The table includes the results for experiment, theory (WinXCOM) and MC simulations (MCNP6, GEANT4 and FLUKA). Once each result is compared to each other, it could be safely stated that the theoretical calculation and all used MC simulations are in well agreement with the experiment since the maximum deviation is found to be as about 6%. These numerical numbers are illustrated in Fig. 5. The biggest MAC value is observed for BaWB-50 sample, and the lowest values is obtained for BaWB-0. In other words, based on the evaluation of MAC values, the best gamma attenuator is BaWB-50 sample. It should be also noted here that the MAC values decrease exponentially by the increase of the gamma energy as expected. In addition, linear attenuation values are further shown in Fig. 6. The order of LAC values for the produced samples is exactly the same as the order of the MAC values.

Another considered parameter in the gamma shielding section of the samples is HVL, which could be easily obtained with help of the measured LAC parameter. Table 3 provides the numerical numbers of the HVL for each considered material. As can be seen easily, with its lowest HVL values, the best gamma attenuator is BaWB-50 sample among the produced composites for each considered gamma energy. Fig. 7 presents the HVL values versus photon energy for the prepared composites. In other words, HVL is a significant parameter for the determination of the gamma attenuation capability of the chosen material. Mostly, in literature, this parameter is compared to other alternative shielding materials at 661.7 keV since many reported work provide the HVL numbers at this certain energy level. The obtained HVL values could be further compared with literature. The HVL values

calculated in this work are could be listed as 3.457 cm, 3.257 cm, 3.098 cm, 2.794 cm, 2.779 cm and 2.543 cm for BaWB-0, BaWB-10, BaWB-20, BaWB-30, BaWB-40 and BaWB-50, respectively. The base polymer matrix without any additive was examined experimentally by Ozkalayci et al. (Özkalaycı et al., 2020). The reported HVL value for the chosen polymer matrix is 6.98 cm, which is 2.74 times greater than the HVL value of BaWB-50 sample at 661.7 keV. Based on these numbers, all samples proposed in the presented study has better gamma shielding capability than the chosen polymer matrix. Therefore, it could be safely stated that addition of barite and/or tungsten boride at any amount improves the gamma shielding capability of the chosen polyester material. Ogul et al. (Ogul, 2022) used the same base polymer matrix and reinforced the matrix with addition of boron and tin, and then, examined the gamma shielding performance of produced samples. They reported that their N-B0Sn50 sample showed the best gamma attenuation capability with 4.572 cm HVL value at 661.7 keV. Based on the reported values, BaWB-0 is even better than N-B0Sn50 material. Rajanna and Ningaiah (2022) produced composites based on isophthalic polyester and doped with WO_3 and investigated their gamma radiation shielding properties at some energies. The HVL values of the ISO+50 wt% WO_3 composite were determined as 2.6, 3.49, 5.63 and 6.19 cm at 356, 662, 1173 and 1332 keV photon energies. In the presented study, these values were calculated as 1.300, 2.469, 3.675 and 3.960 cm for the composite coded as BaWB-50 at the same energies. Considering the HVL results, BaWB-50 composite has 100%, 41.4%, 53.2% and 56.3% better gamma shielding properties compared to ISO+50 wt%WO3 composite at 356, 662, 1173 and 1332 keV energies, respectively. Additionally, Fig. 7 shows the TVL and MFP values versus photon energy for the prepared composites. TVL and MFP graphs convey the same information as the HVL graph.

The following gamma shielding parameter is Z_{eff} values that defines the probability of gamma ray interactions with the considered absorber. Table 4 gives the numerical values of the obtained Z_{eff}, and Fig. 8 illustrates these numbers. It is clear that the parameter decreases exponentially with increase of the gamma energy, and BaWB-50 sample has the biggest Z_{eff} value for each gamma energy. In other words, the interaction probability of gamma rays with BaWB-50 is greater than the rest of the fabricated materials. These interactions make the gamma rays lose their energy while passing through the material, and BaWB-50 material will show better gamma attenuation property.

The second analysis considered for the prepared composites is the determination of neutron attenuation characteristics of the chosen materials. On this purpose, effective neutron removal cross sections of the prepared sample and the simulated neutron numbers passing through the absorbers as a function of neutron energy and material thickness are determined. Table 5 provides the effective neutron removal cross sections of the prepared sample, and it is clearly seen that the highest value (0.0943 cm^{-1}) is obtained with BaWB-50. Based these numbers, it is expected that neutron shielding performance of the prepared materials should be in order of BaWB-50 > BaWB-40 > BaWB-30 > BaWB-20 > BaWB-10 > BaWB-0. In Reference (Ogul, 2022), the validity of GEANT4 for neutron shielding tests is previously discussed, and significant consistency is reported with experiment, FLUKA and MCNP6. Therefore, GEANT4 simulation package is used for further neutron shielding evaluations due to the lack of experimental apparatus. On this regard, Table 6 provides total macroscopic cross sections, mean free paths and number of transmitted neutrons for the produced samples of 10 mm thickness. Here, 10^7 neutrons at 4.5 MeV are sent over the modelled composites. As it is expected from effective neutron removal cross sections, the lowest transmitted neutron numbers are obtained with BaWB-50 material. However, it should be noted here that the difference between the samples are not significant, and the maximum difference is about 1% level. On the other hand, Figs. 9 and 10 illustrate the graphs for the transmitted neutron numbers versus sample thicknesses and neutron energy, respectively.

The mass stopping power (MSP), sometimes referred to as the radiation-stopping power, is the average energy loss per unit path length brought on by bremsstrahlung photon emission. Therefore, the total average energy loss per propagation distance of a charged particle owing to collisions and photon emission determines a material's overall stopping power for that charged particle. In this study, the mass stopping power and predicted range values of the composites BaWB-0, BaWB-10, BaWB-20, BaWB-30, BaWB-40, and BaWB-50 were examined between energies of 0.015 and 15 MeV. As the kinetic energy increases, the MSP values reach a peak and then begin to decline until they reach their minimum value. Figs. 11 and 12 show the proton and alpha MSP values, and both show that the BaWB-0 composite has the highest collision MSP estimates for H^1 and He^{+2} particles. Furthermore, Figs. 11 and 12 indicate that the BaWB-50 has the lowest proton (H^1) and alpha (He^{+2}) MSP values. The amount of H^1 and He^{+2} penetration at a resting location as well as the accessibility of shielding materials are represented by the projected range (PR). The six composite samples were subjected to proton and alpha PR calculations using the SRIM technique, and the results are represented in Figs. 13 and 14, respectively. The BaWB-50 exhibits the lowest PR values for proton (H^1) and alpha (He^{+2}) particles, as seen in Figs. 13 and 14. Additionally, it is obvious that the BaWB-50 sample has the best H^1 and He+2 shielding properties, as the composites with the best shielding materials had the lowest PR values.

4. Conclusion

It is well-known that polyester-based filler doped composites put forward low cost, durable as well as effective photon absorber which may further provide promising upgrade on shielding features. Herewith, barite ad tungsten boride compounds at different proportions in the present study have been exploited as additive filler into unsaturated polyester and evaluated as radiation shields over gamma energy region ranging from 276.4 to 1332.5 keV. The experimental mass attenuation coefficients of the prepared samples have been found in line with those of WinXCOM computer program and MC simulations with help of MCNP6, GEANT4 and FLUKA codes. Based on all shielding parameters, the addition of BaWB filler to polyester material reveals a positive effect for the shielding performance. Thus, BaWB-50 polyester sample with high content of the studied BaWB composites possessessuperior attenuation effectiveness and may be evaluated in the fields required durable and lightweight materials such as medical, spacecraft and so on. In the present study, the shielding capacities of ternary composites containing polyester, barite and tungsten boride, which were not included in the literature, for gamma, neutron and charged particle radiations were extensively investigated. It is seen from the literature review that there is no such comprehensive study in the literature. When the obtained results were examined, it was observed that the produced composites, especially the BaWB-50 sample, had superior ionizing radiation shielding capacity despite the high energies. The present data might contribute significantly to the literature to improve the quality and quantity of shields.

Author statement

F. Akman: Supervision, Validation, Investigation, Resources, Writing-Review&Editing. H. Ozdogan: Writing-Original Draft, Formal analysis, Data Curation. O. Kilicoglu: Writing-Original Draft, Formal analysis, Data Curation. H.Ogul: Writing-Original Draft, Formal analysis, Data Curation. O. Agar: Writing-Original Draft, Conceptualization, Writing-Review&Editing. M.R. Kacal: Methodology, Validation, Formal analysis. H. Polat: Writing-Original Draft, Methodology, Investigation. A. Tursucu: Writing-Original Draft, Investigation.

Declaration of competing interest

There are no conflicts of interest to declare.

Data availability

Data will be made available on request.

References

Abu Saleem R, A., Abdelal, N., Alsabbagh, A., Al-Jarrah, M., Al-Jawarneh, F., 2021. Radiation shielding of fiber reinforced polymer composites incorporating lead nanoparticles—an empirical approach. Polymers 13 (21), 3699.

Agostinelli, S., Allison, J., Amako, K.A., Apostolakis, J., Araujo, H., Arce, P., et al., 2003. GEANT4—a simulation toolkit. Nucl. Instrum. Methods Phys. Res. Sect. A Accel. Spectrom. Detect. Assoc. Equip. 506 (3), 250–303.

Akman, F., Ogul, H., Kaçal, M.R., Polat, H., Dilsiz, K., Agar, O., 2021. Gamma attenuation characteristics of CdTe-Doped polyester composites. Prog. Nucl. Energy 131, 103608.

Akman, F., Ogul, H., Ozkan, I., Kaçal, M.R., Agar, O., Polat, H., Dilsiz, K., 2022. Study on gamma radiation attenuation and non-ionizing shielding effectiveness of niobium-reinforced novel polymer composite. Nucl. Eng. Technol. 54 (1), 283–292.

Al-Hadeethi, Y., Sayyed, M.I., Tijani, S.A., 2019. Gamma radiation attenuation properties of tellurite glasses: a comparative study. Nucl. Eng. Technol. 51 (8), 2005–2012.

Alavian, H., Tavakoli-Anbaran, H., 2019. Study on gamma shielding polymer composites reinforced with different sizes and proportions of tungsten particles using MCNP code. Prog. Nucl. Energy 115, 91–98.

Aloraini, D.A., Almuqrin, A.H., Sayyed, M.I., Al-Ghamdi, H., Kumar, A., Elsafi, M., 2021. Experimental investigation of radiation shielding competence of Bi2O3-CaO-K2O-Na2O-P2O5 glass systems. Materials 14 (17), 5061.

Alothman, M.A., Alrowaili, Z.A., Al-Baradi, A.M., Kilicoglu, O., Mutuwong, C., Al-Buriahi, M.S., 2021. Elastic properties and radiation shielding ability of ZnO–P2O5/B2O3 glass system. J. Mater. Sci. Mater. Electron. 32 (14), 19203–19217.

Alqahtani, M.S., Almarhaby, A.M., Hussein, K.I., AbouDeif, Y.M., Afifi, H., Zahran, H., Yaha, I.S., Grelowska, I., Yousef, E., 2021. Radiation attenuation and photoluminescence properties of host tellurite glasses doped with Er3+ ions. J. Instrum. 16 (1), P01002.

Baştuğ, A., Içelli, O., Gürol, A., Şahin, Y., 2011. Photon energy absorption parameters for composite mixtures with boron compounds. Ann. Nucl. Energy 38 (10), 2283–2290.

Battistoni, G., Boehlen, T., Cerutti, F., Chin, P.W., Esposito, L.S., Fassò, A., et al., 2015. Overview of the FLUKA code. Ann. Nucl. Energy 82, 10–18.

Çakıroğlu, M.A., Kaplan, A.N., Süzen, A.A., 2021. Experimental and DBN-Based neural network extraction of radiation attenuation coefficient of dry mixture shotcrete produced using different additives. Radiat. Phys. Chem. 188, 109636.

Gerward, L., Guilbert, N., Jensen, K.B., Levring, H., 2001. X-ray absorption in matter. Reengineering XCOM. Radiation Physics and Chemistry 60 (1–2), 23–24.

Gong, J.J., Zhang, L., Jia, M.C., Xia, W.M., Chen, J.J., 2018. Study on neutron and photon shielding properties of various concretes using MCNP code. December. In: IOP Conference Series: Earth and Environmental Science, 199. IOP Publishing, 032056. No. 3.

Goorley, T., James, M., Booth, T., Brown, F., Bull, J., Cox, L.J., et al., 2012. Initial MCNP6 release overview. Nucl. Technol. 180 (3), 298–315.

Kara, U., Kilicoglu, O., Ersoy, S., 2020a. Structural and gamma-ray attenuation coefficients of different OAD films for nuclear medicine applications. Radiat. Phys. Chem. 172, 108785.

Kara, U., Kilicoglu, O., Karaibrahimoglu, A., Cavdarli, K., Ince, F., 2020b. Radiation attenuation properties of removable partial dentures (RPD). Mater. Chem. Phys. 253, 123301.

Kilicoglu, O., 2019. Characterization of copper oxide and cobalt oxide substituted bioactive glasses for gamma and neutron shielding applications. Ceram. Int. 45 (17), 23619–23631.

Kilicoglu, O., Mehmetcik, H., 2021. Science mapping for radiation shielding research. Radiat. Phys. Chem. 189, 109721.

Kilicoglu, O., Tekin, H.O., 2020. Bioactive glasses with TiO2 additive: behavior characterization against nuclear radiation and determination of buildup factors. Ceram. Int. 46 (8), 10779–10787.

Kilicoglu, O., Kara, U., Inanc, I., 2021. The impact of polymer additive for N95 masks on gamma-ray attenuation properties. Mater. Chem. Phys. 260, 124093.

Kilicoglu, O., More, C.V., Akman, F., Dilsiz, K., Oğul, H., Kaçal, M.R., Polat, H., Agar, O., 2022. Micro Pb filled polymer composites: theoretical, experimental and simulation results for γ-ray shielding performance. Radiat. Phys. Chem. 194, 110039.

Medhat, M.E., Singh, V.P., 2014. Mass attenuation coefficients of composite materials by Geant4, XCOM and experimental data: comparative study. Radiat. Eff. Defect Solid 169 (9), 800–807.

Nagaraja, N., Sridhar, K.N., Manjunatha, H.C., Vidya, Y.S., Seenappa, L., Gupta, P.D., Ramalingam, H.B., 2022. Measurement of mass attenuation coefficient and its derivable in polymers. Prog. Nucl. Energy 144, 104044.

Ogul, H., 2022. Radiation attenuation properties of polymer composites mixed with tantalum carbide. Radiat. Eff. Defect Solid 177 (5–6), 531–544.

Oğul, H., Polat, H., Akman, F., Kaçal, M.R., Dilsiz, K., Bulut, F., Agar, O., 2022. Gamma and Neutron Shielding Parameters of Polyester-based composites reinforced with boron and tin nanopowders. Radiat. Phys. Chem. 201, 110474.

Ozdogan, H., Kilicoglu, O., Akman, F., Agar, O., 2022a. Comparison of Monte Carlo simulations and theoretical calculations of nuclear shielding characteristics of various borate glasses including Bi, V, Fe, and Cd. Appl. Radiat. Isot. 189, 110454.

Ozdogan, H., Kilicoglu, O., Akman, F., Agar, O., 2022b. Comparison of Monte Carlo simulations and theoretical calculations of nuclear shielding characteristics of various borate glasses including Bi, V, Fe, and Cd. Appl. Radiat. Isot. 189, 110454.

Özkalaycı, F., Kaçal, M.R., Agar, O., Polat, H., Sharma, A., Akman, F., 2020. Lead (II) chloride effects on nuclear shielding capabilities of polymer composites. J. Phys. Chem. Solid. 145, 109543.

Piotrowski, T., Tefelski, D., Polański, A., Skubalski, J., 2012. Monte Carlo simulations for optimization of neutron shielding concrete. Open Eng. 2 (2), 296–303.

Rajanna, A.M., Ningaiah, N., 2022. Polyester-based polymer composites for gamma shielding applications- A substitute for lead. ChemistrySelect 7 (26), e202201214.

Şekerci, M., Özdoğan, H., Kaplan, A., 2019. An investigation on gamma-ray shielding properties of Zr-based bulk metallic glasses. HNPS Advances in Nuclear Physics 27, 48–55.

Shirmardi, S.P., Shamsaei, M., Naserpour, M., 2013. Comparison of photon attenuation coefficients of various barite concretes and lead by MCNP code, XCOM and experimental data. Ann. Nucl. Energy 55, 288–291.

Singh, M., Mudahar, G.S., 1992. Energy dependence of total photon attenuation coefficients of composite materials. Int. J. Radiat. Appl. Instrum. Appl. Radiat. Isot. 43 (7), 907–911.

Singh, M.P., Sandhu, B.S., Singh, B., 2007. Measurement of effective atomic number of composite materials using scattering of γ-rays. Nucl. Instrum. Methods Phys. Res. Sect. A Accel. Spectrom. Detect. Assoc. Equip. 580 (1), 50–53.

Singh, T., Kaur, U., Singh, P.S., 2010. Photon energy absorption parameters for some polymers. Ann. Nucl. Energy 37 (3), 422–427.

Štekl, I., Pospìšil, S., Kovalenko, V.E., Vorobel, V., Leroy, C., Piquemal, F., Eschbach, R., Marquet, C., 2000. Monte-Carlo simulations of neutron shielding for the ATLAS forward region. Nucl. Instrum. Methods Phys. Res. Sect. A Accel. Spectrom. Detect. Assoc. Equip. 452 (3), 458–469.

Tekin, H.O., 2016. MCNP-X Monte Carlo Code Application for Mass Attenuation Coefficients of Concrete at Different Energies by Modeling 3× 3 Inch NaI (Tl) Detector and Comparison with XCOM and Monte Carlo Data. Science and technology of nuclear installations, 2016.

Vahabi, S.M., Bahreinipour, M., Zafarghandi, M.S., 2017. Determining the mass attenuation coefficients for some polymers using MCNP code: a comparison study. Vacuum 136, 73–76.